Supporting Information

Wavelength-Dependent Bifunctional Plasmonic Photocatalysis in Au/Chalcopyrite Hybrid Nanostructures

Xingda An,[1,4] Joshua C. Kays,[2,4] Ian V. Lightcap,[5] Tianhong Ouyang,[1,4] Allison M. Dennis,[2,3,4] and Björn M. Reinhard*[1,4]

[1]Department of Chemistry, [2]Department of Biomedical Engineering, [3]Division of Materials Science and Engineering, and [4]The Photonics Center, Boston University, Boston, MA 02215, USA. [5]Center for Sustainable Energy, University of Notre Dame, Notre Dame, IN 46556, USA.

Correspondence to: bmr@bu.edu

1. Supporting Experimental Procedures

Synthesis of Plasmonic Chalcopyrite Nanocrystals.

Chalcopyrite $CuFeS_2$ nanocrystals (NCs) were synthesized by hot injection according to literature[1] with slight modifications. Equimolar amounts of iron(II) chloride and copper(II) acetate (0.3 mmol each, Sigma-Aldrich, TM grade) were loaded to a 100 mL round bottom flask with a stir bar in an argon-filled glovebox, along with 6 mL of oleic acid (Sigma-Aldrich) and 6mL of octadecene (Sigma-Aldrich). The flask was added to a Schlenk line and heated to 105 °C under vacuum to degas for 30 min. The flask was flushed with argon and heated to 150 °C to dissolve all metal salts, then heated to 180 °C. 3 mL dodecanethiol was injected (causing the solution to change color), and temperature was allowed to recover for 1 min, followed by injection of 3 mL 0.1 M sulfur in oleylamine over 5 min. After this, NCs were left to grow for 10 min then cooled. NCs were cleaned via dilution in hexanes (1:1) and precipitation with ethanol (4-fold excess), followed by centrifugation for 5 min at 21000 rcf. The resulting pellet was then resuspended in chloroform and stored in a sealed 6-dram vial at 4 °C.

Synthesis of Au NSs.

For synthesis Au nanospheres (NSs), a seed solution was first prepared by heating a $HAuCl_4$ water solution (2 mg, 20 mL) to boil, and rapid addition of 0.8 mL 40 mM sodium citrate at high stirring rate. The solution was heated for another 2 min and allowed to cool down, and the color turned from wine to red. A growth solution was prepared by mixing 2.5 mL 60 mM ascorbic acid, 1.25 mL 40 mM sodium citrate, and 10 mL $HAuCl_4$ (20 mg), and then diluting to a total volume of 50 mL with DI water. For NS growth, 15 mL seed solution was first diluted to 100 mL with DI water; then the growth solution was very slowly added with stirring. The size of the NSs was monitored with Dynamic Light Scattering, and when the hydrodynamic diameter reaches 80 nm, the suspension was boiled for 30 min, and its pH was titrated to 7 with 0.01 M NaOH. The colloid was centrifuged, washed three times with DI water, and stored at 4 ^oC for further use.

Preparation of the Hybrid Plasmonic Photocatalyst Controls.

L-NR-NCs were synthesized in a one-pot self-assembly approach as shown in Experimental section in the main text. For preparation of L-Au-NCs and L-Ag-NCs controls, 1 mL colloid of 10^{10} particle/mL 80 nm diameter Au Nanospheres (NSs) suspension as synthesized above, or 40 nm Ag NSs suspension (Nanocomposix) were used. For synthesis of L-NR control, no NC suspension was added in the preparation process, and the rest of the procedures were identical to L-NR-NCs.

Supplemental Structural Characterization Methods of the Hybrid Plasmonic Photocatalyst.

Transmission Electron Microscopy (TEM), Scanning Transmission Electron Microscopy (STEM) and Energy Dispersive X-Ray Spectroscopy (EDX) were performed with a Tecnai Osiris TEM with a Super-X EDX detection system at 200 kV acceleration voltage. Copper/carbon TEM grids (TedPella) were used. For membrane width and NCs lattice calculations, statistics were calculated from 100 micrographs obtained in 5 independent experiments. Scanning Electron Microscopy (SEM) images were obtained on a Zeiss Supra 55 VP SEM at 30 μm aperture and 5 kV EHT.

Microwave Plasma-Atomic Emission Spectroscopy (MP-AES) results were obtained on an Agilent 4200 MP-AES with SPS 4 Auto sampler, with each sample run in quadruplicate in each measurement, and repeated three times. Emission wavelengths of Au (242.795 nm), Au (267.595

nm), Fe (373.486 nm), Fe (371.993 nm), Cu (324.754 nm) and Cu (327.395 nm) were used. For the measurements in **Fig. S6**, the water suspensions of L-NR-NCs or NCs only were first prepared. The water suspensions were then either mixed with NaOH or H_2SO_4 to a final electrolyte concentration of 1 M or 0.5 M, respectively; or was just kept in water at room temperature for different times. The colloids were then centrifuged, and the supernatants were collected for element measurements of the released concentrations from the nanocomposites or NCs. The concentrations obtained at time 0 (right after preparation of L-NR-NCs or redispersing of NCs into water) were set to 0 and used as a baseline.

UV-vis absorbance spectra were collected with a Cary 5000 Spectrometer with a scan rate of 10 nm/s. A 1 cm light path Quartz cell (Starna) and the same L-NR-NCs concentration as measured by MP-AES in **Table S1** was used.

X-Ray Diffraction spectra were acquired on a Bruker D2 Phaser XRD with a 2 mm receiving slit and a 2.5^o Söller slit. XRD spectra in **Fig. 1D** was measured with L-NR-NCs or controls prepared as described above. Interplanar distances in **Fig. 1E** was calculated from Bragg's law with a source wavelength of 1.54 Å. XRD spectra in **Fig. 3B** and **Fig. S11A** were measured with L-NR-NCs prepared with a 10-time NCs concentration as described above to magnify structural changes to the NCs.

XPS was measured on a Nexsa XPS at the Center for Nanoscale Systems (CNS) at Harvard University. Fitting of XPS peaks was performed with XPS PEAK software. A Shirley background and a Pseudo-Voigt function expressed as a weighed sum of Lorentzian and Gaussian functions are used for the fitting of all spectra. Peak percentages are calculated by dividing the peak area of the concerned peak by a sum of that of all peaks fitted in the region.

Supplemental Photoelectrochemical Measurements.

H_2 and O_2 were measured by Thermo Trace gas chromatography with a thermal conductivity detector (GC-TCD) under 1-sun illumination (100 mW cm^{-2}) and with a three-electrode setup where the L-NR-NCs nanocomposites-coated ITO electrodes served as both the photoanode and cathode, and 0.5 M Na_2SO_3 was used as electrolyte. A gas-tight syringe was used to sample the headspace every 6 minutes. For the measurement at 2 hours, a sampling gas volume of 1 mL was used with a total headspace of 37 mL.

9.1 nmol H_2 was detected at 2 hours of measurement from 1 mL sampled air, which leads to 0.337 µmol H_2 in the total 37 mL reaction headspace. The number of electrons related to the produced H_2 can be calculated by #e = 0.337 µmol x 10^{-6} x 6.022 x 10^{23} x 2 = 4.06 x 10^{17}. A 0.6 V external bias was applied in the measurement, the charge can be calculated by multiplying the current of L-NR-NCs in Na_2SO_3 electrolyte of 0.126 mA, calculated from the current density in the 1st light cycle at 0.6 V (vs Ag/AgCl) in Na_2SO_3 of 3.6 mA/cm^2 (**Fig. S14C**) and a surface area of 0.035 cm^2, and the time of measurement (7200 seconds), a charge of 0.91 C could be calculated. The energy in Joules could be calculated by multiplying 0.6 V applied bias with the charge as calculated (0.70 C), and the number of electrons can be derived by converting Joule to eV. The theoretical number of electrons from the system could be calculated as 3.40 x 10^{18}. Thus, the Faradaic Efficiency could be derived by dividing the actual and the theoretical number of electrons, which leads to 11.9%.

Current density (mA cm^{-2}) was calculated from the measured current and the calculated total geometric surface area (SA) of the L-NR-NCs nanocomposites or controls. All control groups

were prepared to contain the same Au and/or NC concentrations as in L-NR-NCs. For the particulate photocatalyst, the calculated geometric surface area gives a conservative estimation of the current densities and photocurrent densities. 10 μL L-NR-NCs colloid with a Au concentration of 70453.4 ppb calculated from MP-AES measurements (**Table S1**) was drop-casted on GC electrodes for PEC measurements, which gives a mass of 7.045 x 10^{-7} g Au. With a mass density of Au NRs of 19.32 g cm^{-3}, and the volume of an individual Au NR of 1.862 x 10^5 nm^3 calculated from the NR length (123 nm) and width (47 nm), the number of L-NR-NCs composite is calculated as 1.958 x 10^8. Considering the area of an individual rod of 1.816 x 10^4 nm^2, SA amounts to 0.035 cm^2. For L-NR control, the same SA was used. For NCs only, the glassy carbon surface area of 0.07 cm^2 was used. For L-Au-NCs and L-Ag-NCs, the Au (diameter of 80 nm) and Ag (diameter of 40 nm) concentrations were controlled to be similar to that in L-NR-NCs, and a surface area of 0.027 cm^2 and 0.10 cm^2 were calculated, respectively. The former is used as SA for L-Au-NCs; since the latter is larger than an effective glassy carbon area of 0.07 cm^2, 0.07 cm^2 is used for L-Ag-NCs.

Photocurrent densities (J_{photo}, mA cm^{-2}) were calculated by subtracting the current densities in dark from those measured with illumination. Conversion between Reversible Hydrogen Electrodes and Ag/AgCl reference electrode is based on: E(vs RHE) = E(vs Ag/AgCl) + 0.059pH + E^e (vs Ag/AgCl), where the E^e (vs Ag/AgCl) = 0.1976. Tafel Plots are constructed based the Tafel Equation:

$$\eta = A \times ln\frac{i}{i_0} \qquad \textbf{Eq. S1}$$

where A is the Tafel Slope; i is current density; i_0 is exchange current density, the current at equilibrium and therefore the x-axis intercept in a Tafel Plot, and η is the overpotential. A Tafel Plot is constructed based on the Linear Sweep Voltammetry curves and reflects the electrochemical kinetics relating the rate of reactions to potentials. It is a plot of the potentials around reaction onset against the log scale of current density. A smaller Tafel Slope is typically associated with more favorable intrinsic kinetics for the catalysis of the reactions of interest. Applied Bias Photon-to-Current Efficiency (ABPE) (Ref. 60 of the main text) is calculated from the LSV curve based on **Eq. S2**:

$$\text{ABPE} = \frac{J_{photon} \times (1.23 - |V_b|)}{I} \qquad \textbf{Eq. S2}$$

where V_b is the applied bias vs RHE, and I is the illumination power density (measured to be 0.946 mW cm^{-2}).

For measurement of the temperature increase at the electrode surface over the 6-hour CA measurements (**Fig. S9A**), a Digi-Sense thermocouple was placed in contact with the GC working electrode surface, and identical measurement conditions were used as described above respectively for NaOH, NaOH + SR, and sulfuric acid electrolytes. Temperature readouts were collected at times 0, 10, 30, 60, 120, 180, 240, 300 and 360 min; and change in temperature versus time 0 was plotted.

Calculation of the Plasmonic Photothermal Temperature Increase.

The temperature increase of a metal particle with different shapes upon illumination can be calculated based the following equation **Eq. S3** (Ref. 57 from main text):

$$\Delta T = \frac{Q}{4\pi K_s R_{eq} \beta} \quad \textbf{Eq. S3}$$

K_s is the thermal conductivity of surrounding medium; for lipid bilayer water suspensions, K_s have been reported to be close to 0.46 W m^{-1} K^{-1}.[2] R_{eq} is the equivalent radius of a nanosphere that possess the same volume as the NR; with length D=123 nm and width d=47 nm for the Au NR, R_{eq} = 35.4 nm. β is a shape factor and for NRs, $\beta = 1 + 0.96587\ln^2(D/d) = 1.894$. Q is absorbed heat power and can be calculated by multiplying the NPs absorption cross section (σ_{abs}) with the irradiance light power density (I) (**Eq. S4**):

$$Q=\sigma_{abs} I \quad \textbf{Eq. S4}$$

The absorption cross section of Au NRs with similar size and aspect ratio as used in our work has been previously reported to be around 5000 nm^2 at 530 nm.[3] The 530 nm LED possess an incident power density (I) of 9.46 W/m^2; and Q could be calculated accordingly to be 4.73 x 10^{-14} W. By plugging Q, R, β, K_s into **Eq. S3**, a temperature increase of ΔT = 1.22 x 10^{-7} K is obtained.

Calculation of temperature increase induced by the chalcopyrite NCs can be performed based on the approach reported in Ref. 43 of the main text. The photothermal transduction efficiency, η, is determined by **Eq. S5**:

$$\eta = \frac{hS\Delta T - Q_{dis}}{P(1-10^{-A})} \quad \textbf{Eq. S5}$$

where hS refers to the thermal conductance, and for a water suspension, it was calculated in Ref. 43 as 0.012 W/K; NC_{is} is the dissipated heat, and was calculated to be 0.028 W in Ref. 43; P is the incident power, and in this work, it can be calculated by multiplying the power density of 9.46 W/m^2 and the electrode area of 7x10^{-6} m^2; A is the absorbance for the L-NR-NCs nanocomposite at 530 nm, A = 1.4. At 808 nm, η of the NCs was determined to be 46% in previously. Assuming the same efficiency at 530 nm, ΔT = 2.33 K is obtained from **Eq. S5**.

Calculation of the Charge Injection Efficiency.

The charge separation efficiency (η_{sep}) of L-NR-NCs is calculated based on the LSV curve in 1 M NaOH + 0.5 M SR with green light (**Fig. 5A**), and **Eq. 5** in the main text, in a slightly modified approach as shown in Ref. 72 of the main text. In the presence of the SR, η_{inj} can be assumed to be 100% (Ref. 72). Thus, $\eta_{sep} = J_{photo} / J_{abs}$. To determine the theoretical photocurrent (J_{abs}) based on light absorption, the light harvesting efficiency (LHE) is first calculated based on absorbance (α(λ)) at different wavelengths in the absorbance spectrum:

$$\text{LHE}(\lambda) = 1 - 10^{-\alpha(\lambda)} \quad \textbf{Eq. S6}$$

J_{abs} can then be calculated according to **Eq. S7-S9** based on the current flux (J_{flux}), which is derived from the photon flux (N_{ph}), the energy of a photon (hv); and the wavelengths at absorption half widths (λ_1 = 499 nm, λ_2 = 551 nm) determined from the absorbance spectrum. N_{flux} is obtained by normalizing the emission spectrum of the 530 nm LED (Thorlabs) with the maximum flux of 9.46 μW/mm^2.

$$N_{ph} = \int_{\lambda_1}^{\lambda_2} N_{flux}(\lambda) \times LHE(\lambda) d\lambda \quad \textbf{Eq. S7}$$

$$J_{flux}(\lambda) = \frac{eN_{ph}(\lambda)}{h\upsilon(\lambda)} LHE(\lambda) \qquad \textbf{Eq. S8}$$

$$J_{abs} = \int_{\lambda_1}^{\lambda_2} J_{flux}(\lambda) d\lambda \qquad \textbf{Eq. S9}$$

A J_{abs} = 799 mA/cm^2 is determined from the equations.

2. Supporting Data Items.

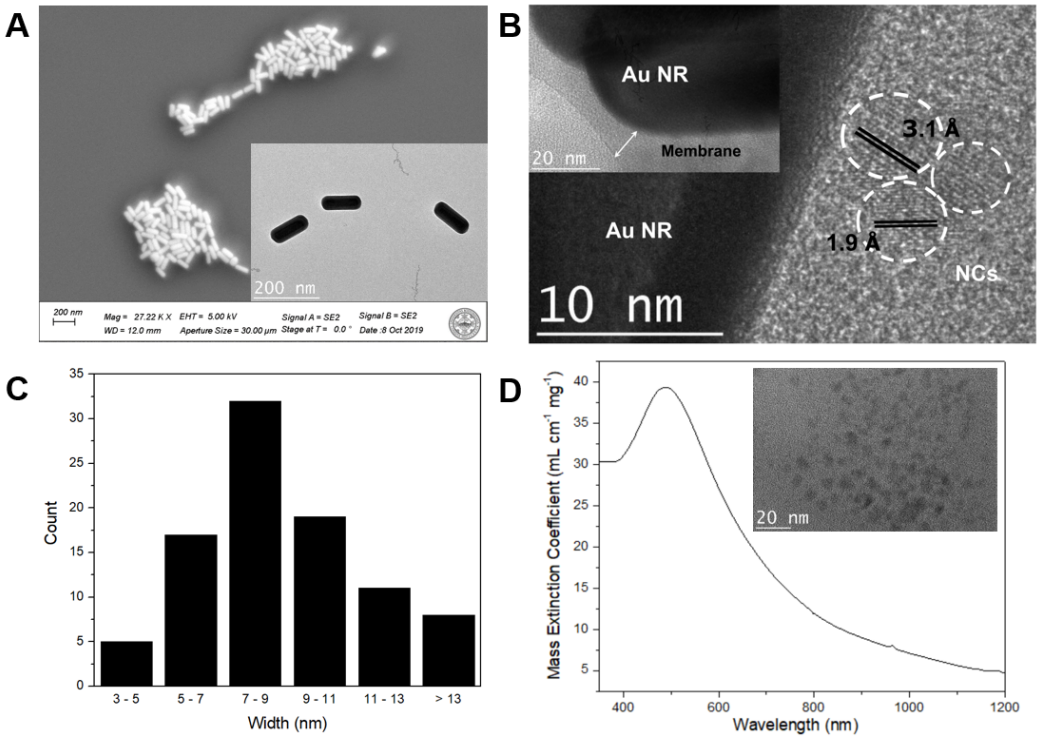

Figure S1. Supporting Characterization of the Au NRs, Hybrid Plasmonic Photocatalyst, and NCs.
(A) SEM and TEM (inset) images of the Au NRs. An average length of 122.9 ± 12.9 nm and width of 46.9 ± 5.9 nm (aspect ratio = 2.62) are measured from 50 NRs.
(B) Supplemental TEM micrographs of the hybrid plasmonic photocatalyst (L-NR-NCs).
(C) Statistical distribution of the lipid membrane width calculated from TEM images of 100 nanocomposite particles.
(D) Absorbance spectra with mass extinction coefficient calculation of the NCs. Inset: TEM micrograph of the NCs. An average NCs diameter of 5.1 ± 0.4 nm is calculated.

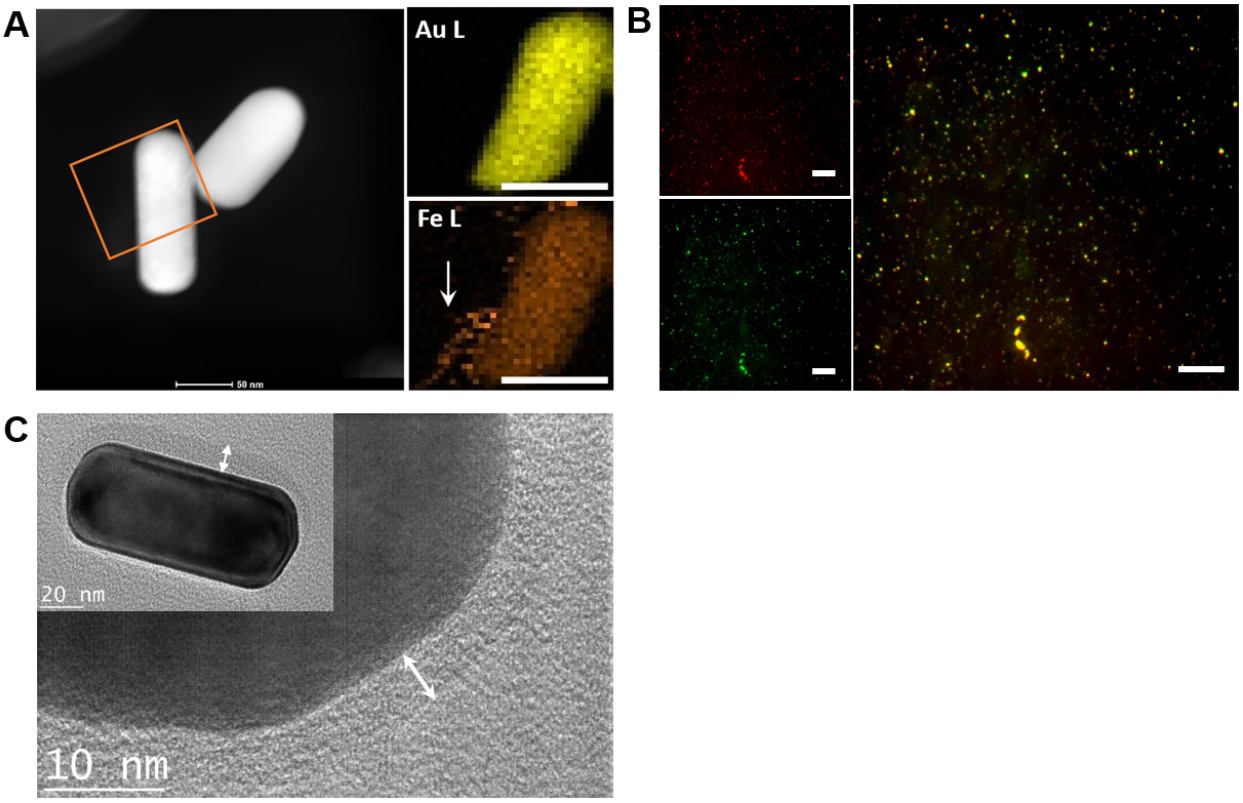

Figure S2. Supporting Characterization of the Hybrid Plasmonic Photocatalyst and Controls.
(A) STEM image (left) and EDX element maps of Au (top right) and Fe L edge (bottom right) of an L-NR-NCs nanocomposite. Orange rectangle: mapped area. Scale bars = 50 nm.
(B) Correlated darkfield (top left), fluorescence (bottom left) images and a channel merge (right) of the L-NR-NCs with a small amount of membrane dye. A high degree of spatial colocalization between the DF signal from the NR cores and the FL signal from the membrane dye is observed, which indicates successful nanocomposite formation. High Manders correlation coefficients M_1 (correlation of DF signals with FL) =0.61 ± 0.02 and M_2 (correlation of FL with DF) =0.63 ± 0.06 are calculated. Scale bars = 10 μm.
(C) TEM micrographs of lipid-wrapped Au NRs control (L-NR) without any NCs. A visible lipid membrane is observed around the Au NRs (white arrows), yet no EM contrast from the NCs or NCs crystal lattices can be detected.

Table S1. Summary of Element Concentrations from MP-AES Measurements

Group	Au Concentration (ppb)	Cu Concentration (ppb)	Fe Concentration (ppb)
NCs stock solution	-	18191.5±825.2	39353.9±1951.5
L-NR-NCs	70453.4±5705.2	2301.8±384.6	4169.4±1143.1

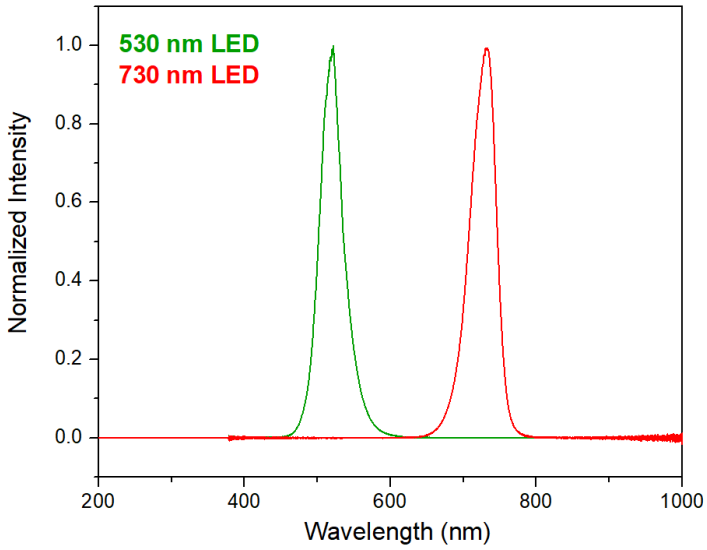

Figure S3. Spectra of LEDs Used for Illumination in This Work.
Spectra obtained from Thorlabs (https://www.thorlabs.com/newgrouppage9.cfm?objectgroup_id=2692).

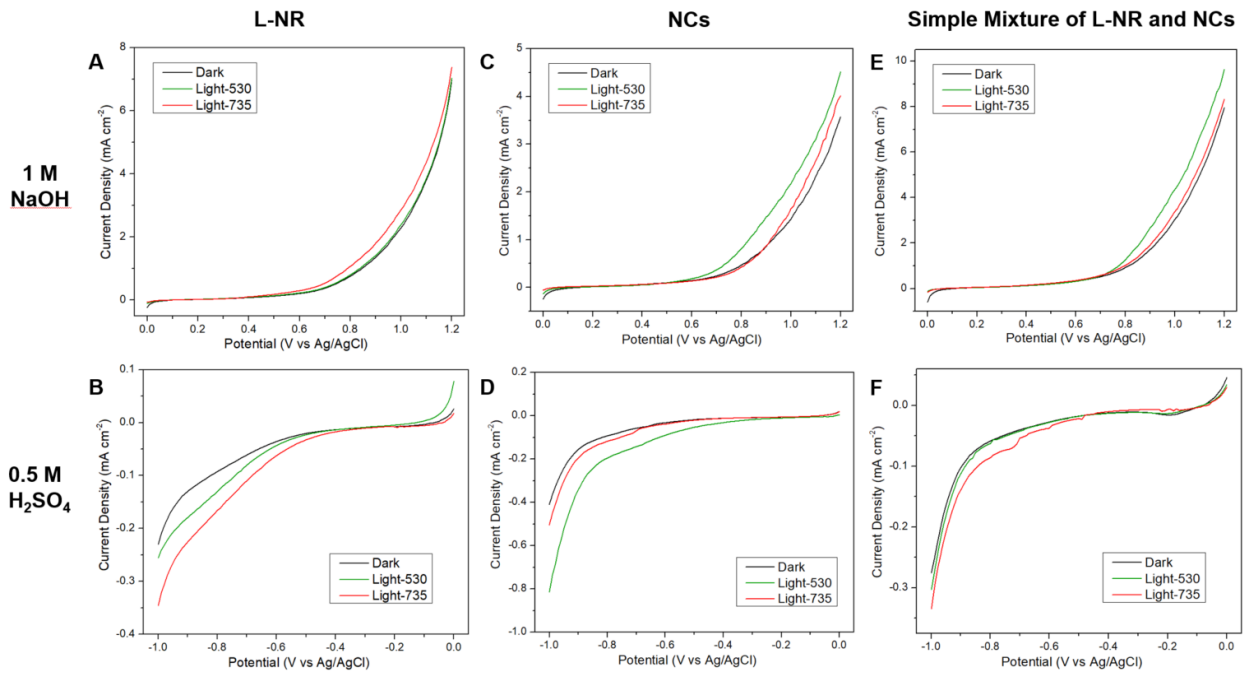

Figure S4. Photoelectrochemical Characterization for Control Groups.
(A-F) LSV curves for lipid-wrapped Au NRs control (L-NR) without the NCs (A, B), NCs only (C, D), and a simple mixture of L-NRs and NCs (E, F) in 1 M NaOH (top row) or 0.5 M H_2SO_4 (bottom row), measured after 100 cycles of activation in dark (black), with green-light illumination of a 530 nm LED or red-light illumination of a 730 nm LED.
In the L-NR control, poor catalytic performance is observed in both electrolytes; since the longitudinal LSPR mode for the Au NRs around 745 nm possess larger absorption cross-section than the vertical mode around 510 nm, red-light illumination produced a larger light response in both electrolytes. For NCs only, in both electrolytes, green-light illumination more efficiently excites the plasmon resonance mode and induced larger light responses. None of these conditions for the two control groups showed comparable J_{photo} to L-NR-NCs. For the simple mixture control, a wavelength-dependent light response can be observed similar to L-NR-NCs, as green light led to a more evident increase in OER current density in alkaline electrolyte, while red light induced slightly larger J_{photo} in acid. However, the current density or light response in the simple mixture control are not nearly comparable to that achieved by L-NR-NCs, due to a lack of spatial correlation between the NRs and NCs for resonant enhancement as well as for charge transfers.

Table S2. Summary of Onset and Potential at 10 mA cm^{-2} for L-NR-NCs and Controls.

Group	1 M NaOH		1 M NaOH + 0.5 M SR		0.5 M H_2SO_4	
	Onset Potential (V vs Ag/AgCl) [a]	Potential at 10 mA cm^{-2} (V vs Ag/AgCl)	Onset Potential (V vs Ag/AgCl)	Potential at 10 mA cm^{-2} (V vs Ag/AgCl)	Onset Potential (V vs Ag/AgCl)	Potential at 10 mA cm^{-2} (V vs Ag/AgCl)
L-NR-NCs Dark	0.48	- [b]	0.32	0.66	-0.36	-
L-NR-NCs Light 1st Scan	**0.28**	**0.97**	**0.20**	**0.36**	**-0.27**	**-**
L-NR-NCs Light 100th Scan	**0.10**	**0.88**	**0.14**	**0.32**	**-0.56**	**-0.83**
L-NRs Light (100th scan)	0.42	-	0.18	0.41	-0.69	-
NCs only Light (100th scan)	0.51	-	0.69	-	-0.76	-
Simple Mixture Light (100th scan)	0.36	-	0.22	0.50	-0.74	-

[a]Calculated as the potential where the current density reached 0.1 mA cm^{-2};

[b]All "-" in this table indicates that this group did not reach 10 mA cm^{-2}.

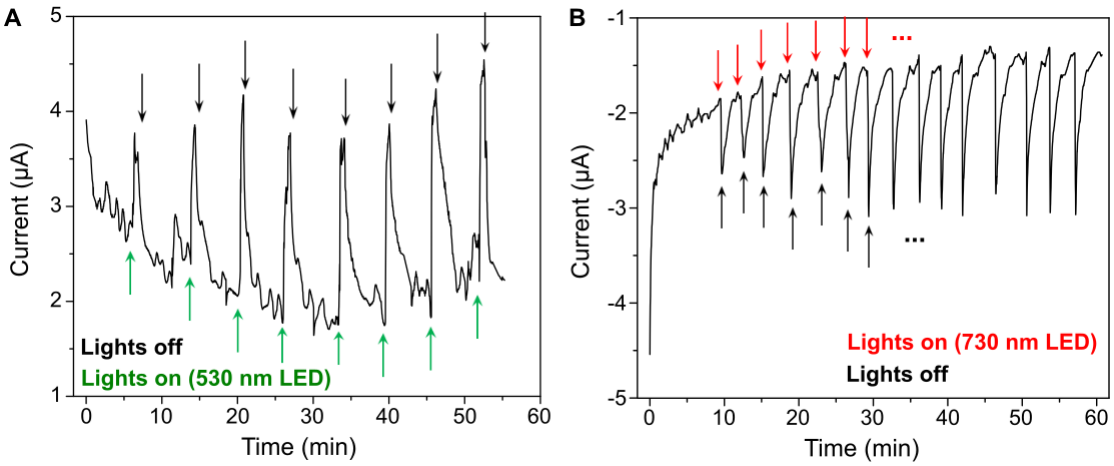

Figure S5. Photocurrent Measurement of L-NR-NCs Light Response.
(A-B) Photocurrent measured from chronoamperometry scans with an applied bias of 0 V (vs Ag/AgCl) NCs in 1 M NaOH electrolyte with or without 530 nm LED illumination (A) or in 0.5 M H_2SO_4 electrolyte with or without 730 nm LED illumination (B). In both cases, steady photocurrent of around 2 μA over an hour of measurement of multiple on/off cycles was observed.

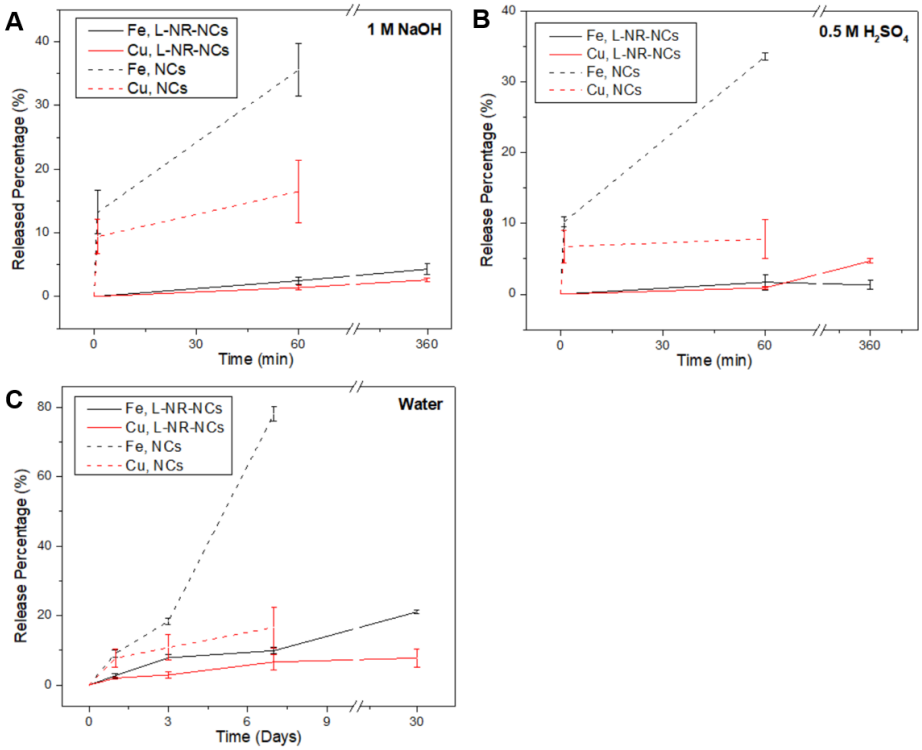

Figure S6. MP-AES Measurement of Fe and Cu Release from L-NR-NCs or NCs.
(A-C) Percentages of Fe (black) and Cu (red) concentrations in supernatants of L-NR-NCs (solid) or NCs only (dashed) after different times of treatment in 1 M NaOH (A), 0.5 M H_2SO_4 (B), or different times of storage in just the water suspension (C). Supernatant Fe and Cu concentrations at time 0 are used as a baseline; and percentages are calculated by dividing the measured supernatant concentrations (after centrifuge separation of L-NR-NCs or NCs) by the total concentration of the colloids at Day 0. Error bars: Mean ± standard deviation of 3 independent measurements.
Significantly higher released concentrations for both elements are recorded for NCs only than for the L-NR-NCs, corroborating that the lipid-wrapped hybrid nanocomposite provides great stability both in the electrolyte solutions, and in water over long-term storage. In all groups, a preferential dissolution of Fe is seen over Cu. This is consistent with previous reports,[4] and could be due to the reduction of Fe(III) and preferential release of Fe(II) (Ref. 56 in the main text); besides, oxidation of Cu(I) to form CuO in alkaline medium and water could also decelerate the dissolution of Cu(II).

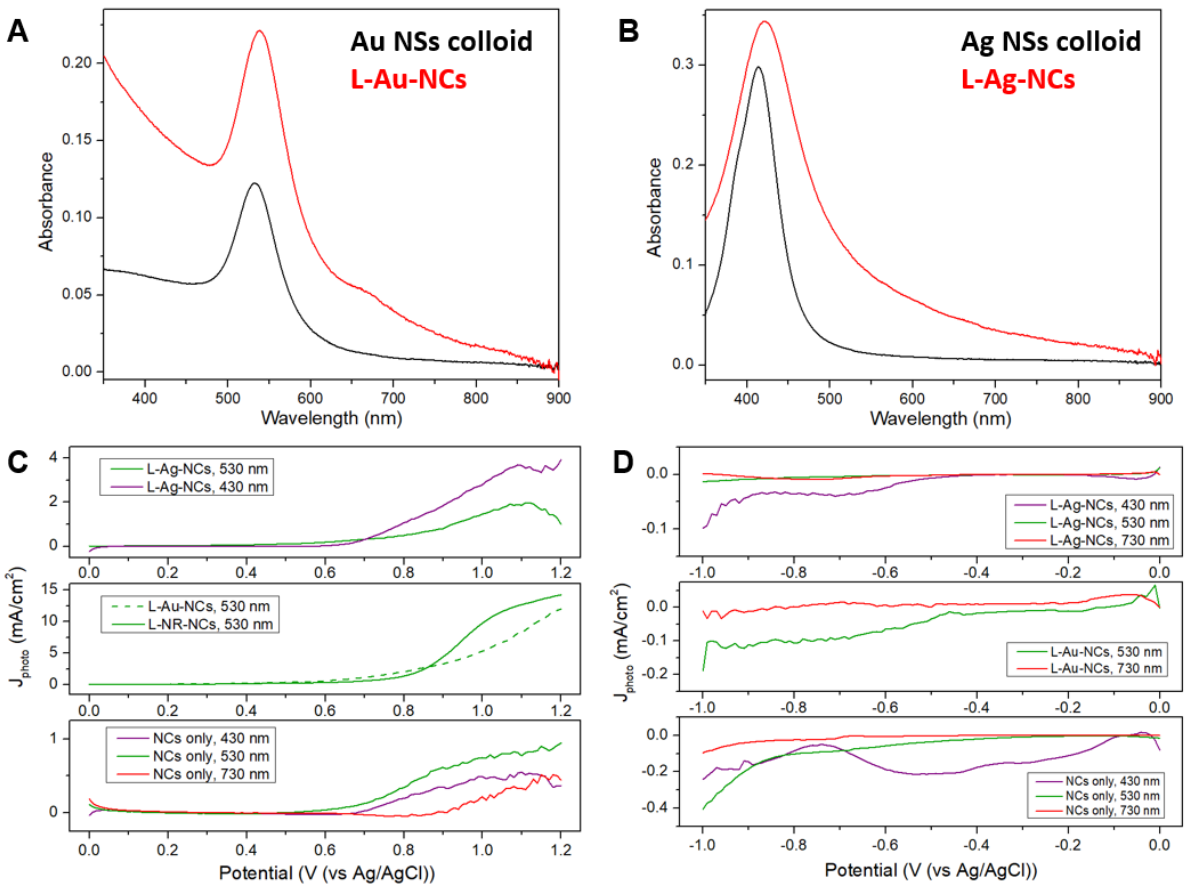

Figure S7. Supporting Characterization of the Plasmonic Photocatalytic Mechanism.
(A, B) UV-vis absorbance spectra of L-Au-NCs (A) and L-Ag-NCs (B) controls (red curves) prepared with Au or Ag nanospheres (NSs) (black curves) at the same metal and NCs concentration as in L-NR-NCs. Strong resonant absorption enhancement in the NCs plasmon resonance region between 500 and 550 nm is observed for L-Au-NCs due to a spectral overlap of NCs and Au NSs LSPR; whereas only a slight gain and broadening in the resonance peak is seen in L-Ag-NCs, because of a less degree of spectral overlap with the Ag NSs LSPR around 420 nm.
(C) Photocurrent density (J_{photo}, measured by subtracting dark curve from light curve) curves for L-NR-NCs, L-Ag-NCs or L-Au-NCs controls, and the NCs only control in 1 M NaOH with different excitation wavelengths. Early onset and high J_{photo} are observed in both L-NR-NCs and L-Au-NCs due to the resonant plasmonic enhancement by both Au NRs and Au NSs. L-Ag-NCs showed very low J_{photo} similar to that observed for NCs only control (see also **Fig. S4C**), indicating that the lack of a spectral overlap between Ag NSs and NCs is insufficient to provide any plasmonic enhancement.
(D) J_{photo} curves for L-Ag-NCs or L-Au-NCs controls and NCs only control in 0.5 M H_2SO_4 with different illumination wavelengths. L-Ag-NCs (top) are illuminated respectively with 530 nm, 730 nm, and a 430 nm LED for the LSPR of Ag cores; L-Au-NCs are tested with 530 and 730 nm. In none of these conditions did the controls record comparable J_{photo} compared to that of the hybrid plasmonic photocatalyst L-NR-NCs (see **Fig. 2E**), which is due to a lack of a distinct plasmon resonance mode in the controls that do not overlap with the NCs LSPR that induces electron transfer from the metal cores to the NCs for HER. This finding necessitates the choice of Au NRs in the hybrid plasmonic photocatalyst L-NR-NCs.

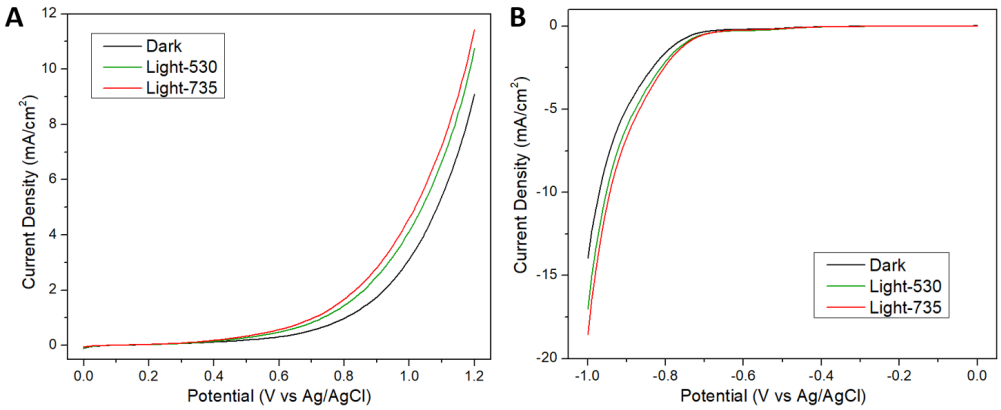

Figure S8. Photoelectrochemical Characterization for Au NRs Control.
(A-B) LSV curves for Au NRs control not coated with the hybrid membrane and without the NCs in 1 M NaOH (A) or 0.5 M H_2SO_4 (B), measured after 100 cycles of activation in dark (black), with green-light illumination of a 530 nm LED or red-light illumination of a 730 nm LED.
Very low light response is observed for Au NRs control in both electrolytes. However, an earlier onset and larger current density is recorded for Au NRs control in dark compared to the dark curves of the L-NRs control (**Fig. S4A, B**), which evidences the shielding effect of the lipid membrane.

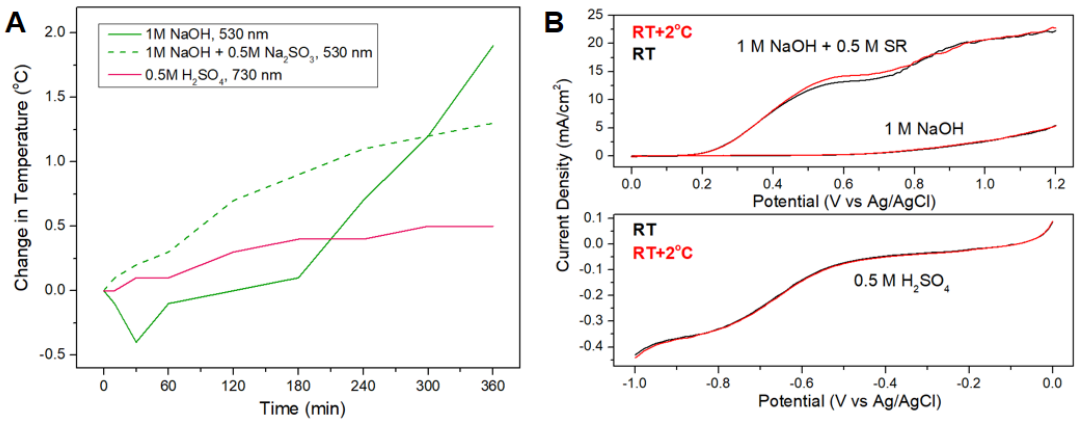

Figure S9. Characterization of the Effect of Temperature on Catalysis.
(A) Measurement of temperature change on the glassy carbon electrode surface during chronoamperometry (CA) measurements for L-NR-NCs in 1 M NaOH with 530 nm illumination and 0.8 V applied bias vs Ag/AgCl (green, solid), in 1 M NaOH + 0.5 M SR with 530 nm illumination and 0.8 V applied bias (green, dashed), or in 0.5 M H_2SO_4 with 730 nm illumination and -0.7 V applied bias (red). In all cases, only a minor temperature increase close to or less than 2 °C is measured over 6 hours.
(B) LSV curves for L-NR-NCs in dark in different electrolytes at room temperature (black) versus with an electrolyte temperature that is 2 °C above the room temperature. Negligible changes are observed in all electrolytes in terms of onset potentials and current densities, which indicate that the measured temperature increase around 2 °C in (A) is unlikely to cause a major change in the catalytic properties of L-NR-NCs, and it's indeed a light-induced charge transfer and Cu-mediated effect that led to the onset in current densities observed in our PEC characterizations.

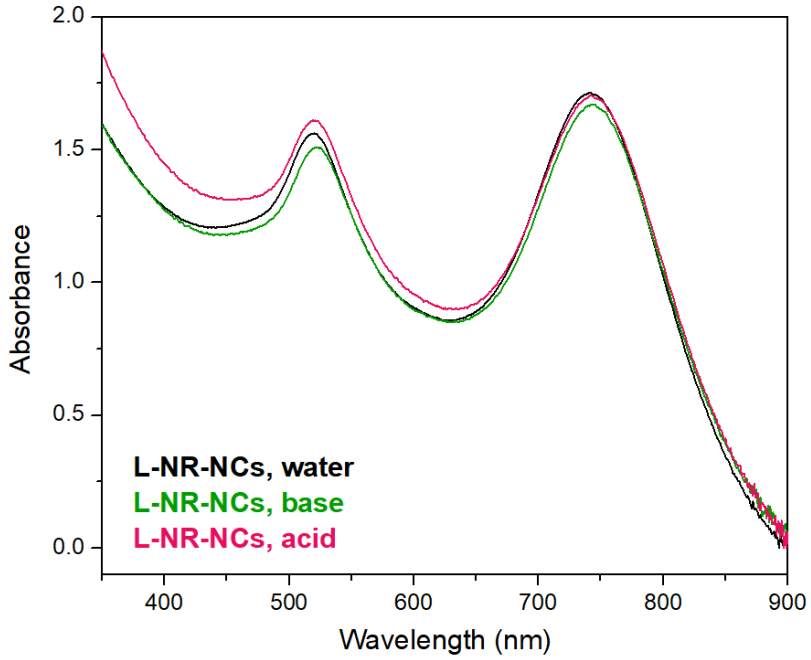

Figure S10. UV-Vis Absorbance Spectra of L-NR-NCs Aqueous Suspensions.

L-NR-NCs suspensions in water (black), 1 M NaOH (green), and 0.5 M H_2SO_4 (red) show overall similar resonance peaks, indicating that the structure of the nanocomposite is preserved in all three suspensions. Notably, for the spectrum of the suspension in NaOH (green curve), a decrease in the intensity for both resonance peaks as well as a red-shift in the peak wavelengths are observed compared to the curve in water. This is consistent with the Cu(I) oxidation and the Cu(II) oxide formation in base discussed in the main text, which can lead to an increase in the refractive index around the NCs in the nanocomposite, as well as reduction of the contribution from the plasmonic chalcopyrite nanocrystals and its absorbance. The spectra in water and in acid show similar wavelengths for both resonance peaks. The high-energy feature around 510 nm is increased in acid. This could be due to a removal of oxides that were formed during the preparation processes, which then reveals the plasmonic NCs for increased absorption due to the LSPR around 500 nm as well as due to interband transition at even higher energies.

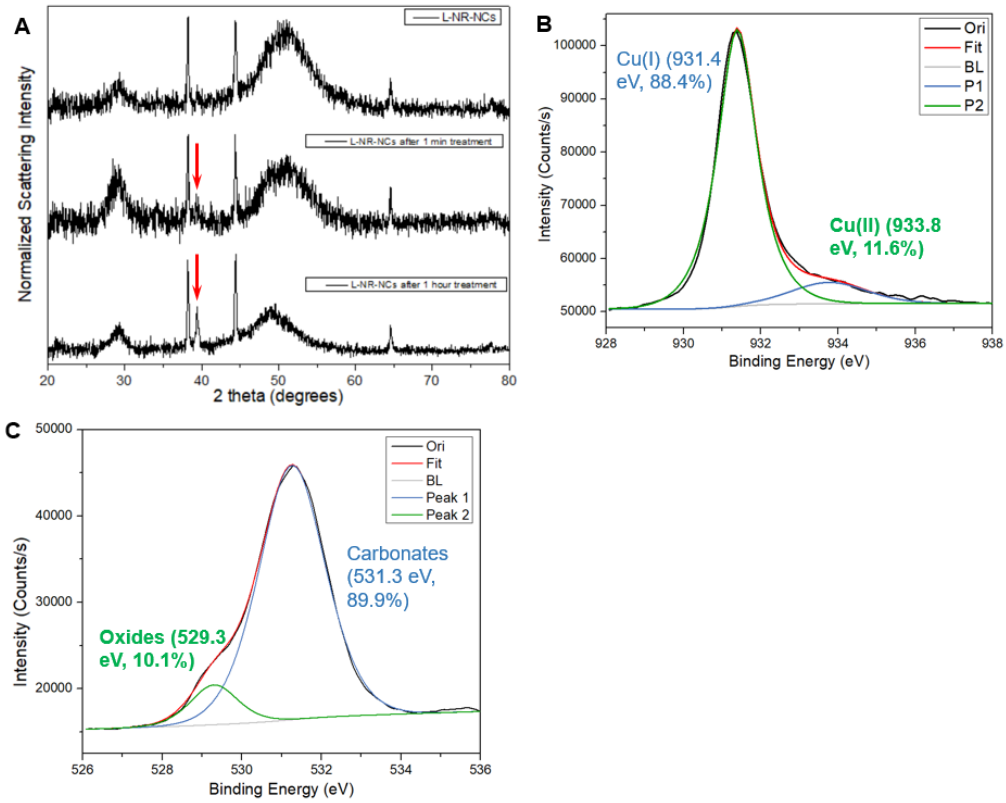

Figure S11. Supporting Characterization of the Cu(I)/Cu(II)-Mediated Catalytic Mechanism.
(A) XRD spectra of a L-NR-NCs thin film with a 10x higher NCs input concentration than in the PEC measurements before treatment (top), after 1 min (middle) and after 1 hour (bottom) scanning in 1 M NaOH, with the same conditions as used in OER measurements. An increasing trend in the peak intensity of CuO (111) diffraction at $2\theta = 39^{o}$ is observed (red arrow), indicating that the oxidation take place continuously as scanning went on in the alkaline electrolyte with a positive bias.
(B, C) Cu $2p_{3/2}$ (B) and O 1s (C) XPS spectra of NCs after scanning in 0.5 M H_2SO_4 for 1 min with red light illumination, under the same applied bias as the HER measurements. Slightly reduced Cu(II) (11.6%) as well as oxides population (10.1%) to before any treatment (Cu(II): 12.9%, oxides: 10.7%) is recorded, which indicates that scanning in acid leads to a reduction of the formed surface Cu(II) oxides on NCs, and supports our proposed Cu(I)/Cu(II)-mediated catalysis mechanism for HER.

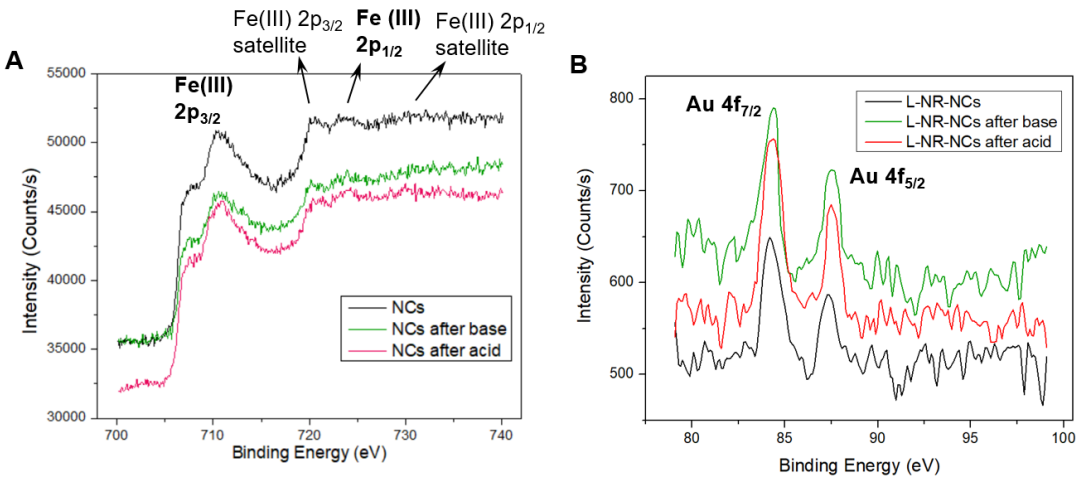

Figure S12. Supporting XPS Characterizations for Fe and Au.
(A) Fe XPS spectra of NCs before any treatment (black), after scanning in 1 M NaOH with green light and identical applied bias as in OER measurements (green) or after scanning in 0.5 M H_2SO_4 with red light and identical applied bias as in HER measurements (red). No significant changes in Fe XPS signals could be observed under these conditions.
(B) Au XPS spectra of L-NR-NCs before any treatment (black), after scanning in 1 M NaOH with green light and identical applied bias as in OER measurements (green) or after scanning in 0.5 M H_2SO_4 with red light and identical applied bias as in HER measurements (red). No significant changes in Au XPS signals could be observed under these conditions.

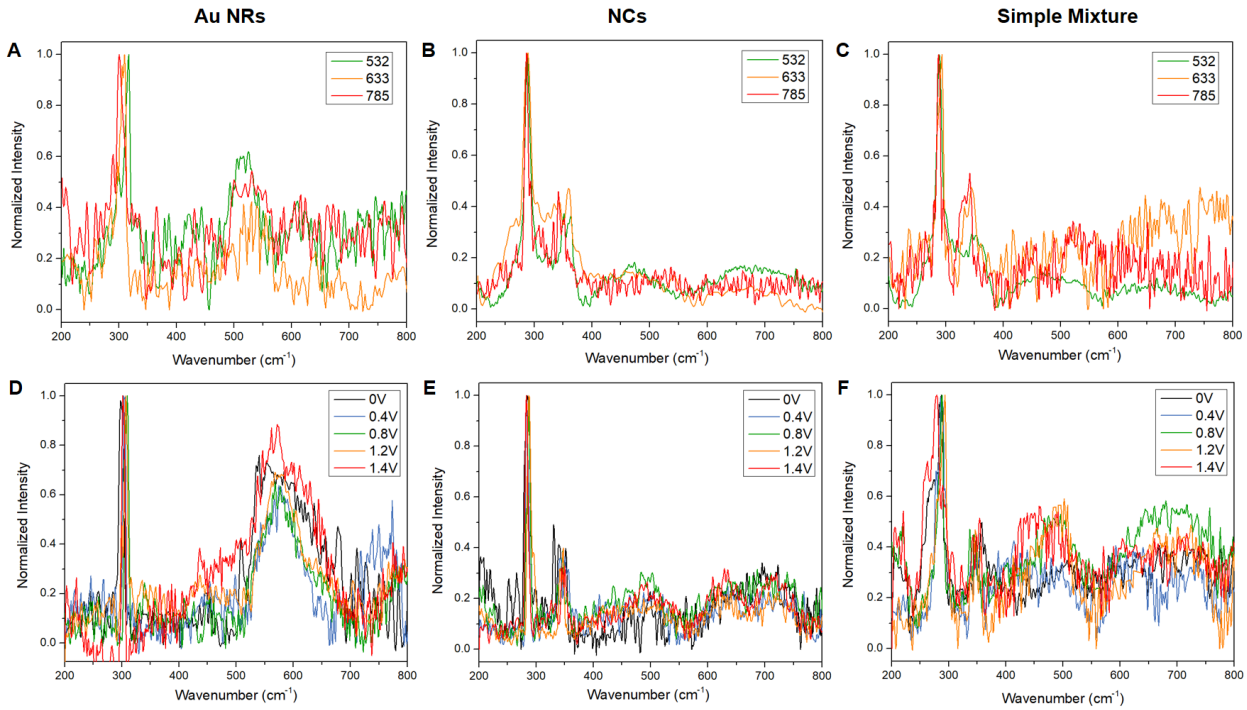

Figure S13. Raman Characterization of the OER Catalytic Mechanism of Control Groups.
(A-C) Raman spectra of drop-casted thin films of control groups Au NRs only (A), NCs only (B) and a simple mixture of Au NRs and NCs (C) at different excitation wavelengths of 532 nm (green), 633 nm (orange) and 785 nm (red).
(D-F) Raman spectra of drop-casted thin films of control groups Au NRs only (D), NCs only (E) and a simple mixture of Au NRs and NCs (F) on ITO substrate with different applied bias in the range of 0 - 1.4 V. All spectra were collected with 532 nm excitation.

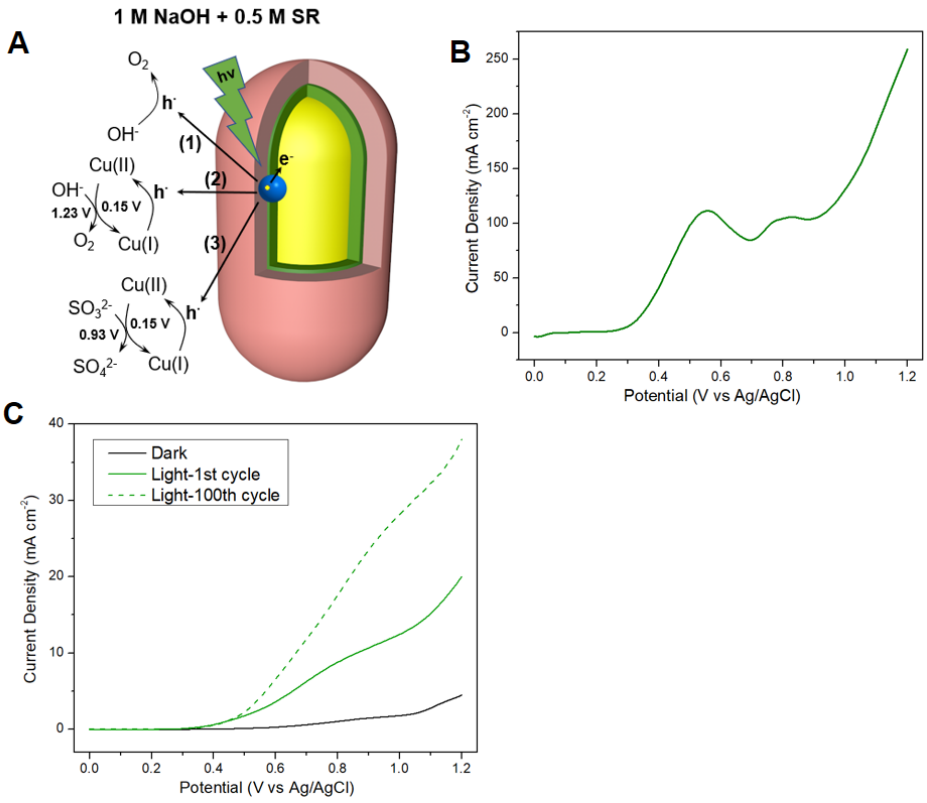

Figure S14. Characterization of Plasmonic Photocatalytic Mechanism with the Sacrificial Reductant. (A) Scheme of the charge transfer and redox processes for L-NR-NCs in 1 M NaOH + 0.5 M SR with green light illumination from a 530 nm LED. (1) Direct plasmonic charge carrier-induced photocatalysis; (2) Cu(I)/Cu(II)-mediated OER catalysis; (3) SR oxidation coupled to Cu(II) for replenishment of Cu(I).
(B) LSV curve of L-NR-NCs in 1 M NaOH + 0.5 M SR with green light illumination from a 530 nm LED acquired after 12 hours of constant CA measurement with an applied bias of 0.8 V (vs Ag/AgCl). After a long-time performance, the current density in the LSV curve decreases moderately compared to the 100th LSV cycle with the same illumination condition (**Fig. 5A**), and the sulfite oxidation peak (around 0.55 V) and the Cu(I) oxidation peak (around 0.8 V) decoupled. The presence of an evident Cu(I) oxidation to Cu(II) peak confirms that the SR successfully replenishes the Cu(I) oxidation state.
(C) LSV curves of L-NR-NCs in 0.5 M SR only electrolyte with green light illumination from a 530 nm LED.

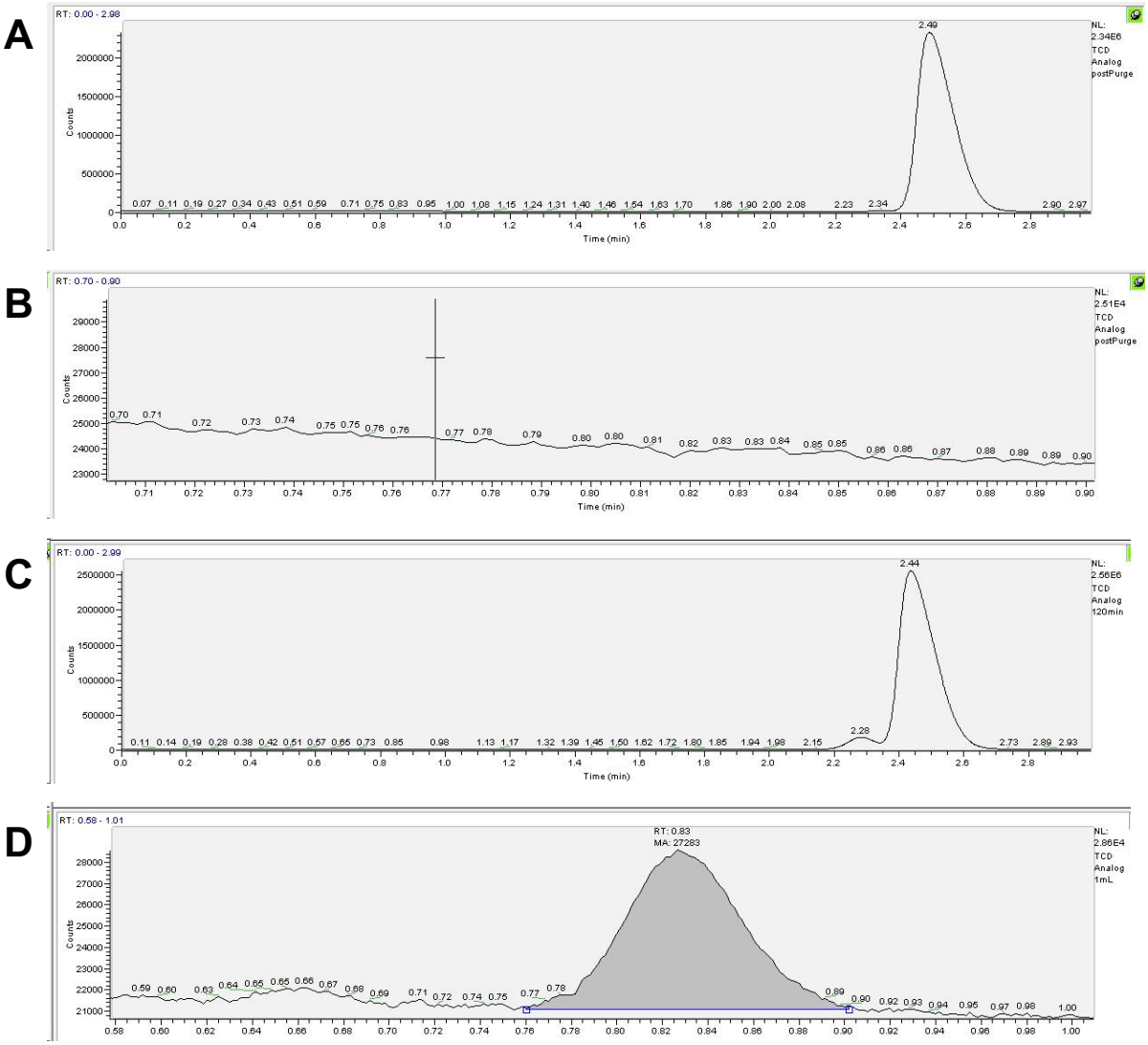

Figure S15. H_2 and O_2 Measurements by GC-TCD.
(A-B) O_2 (A) and H_2 (B) measurement at time 0. No obvious H_2 or O_2 could be measured at the start of the reaction as expected. N_2 gas that was used to purge the cell was detected at retention time of 2.49 min. (C-D) O_2 (C) and H_2 (D) measurement at 120 min. O_2 was measured with a 40 µL sampling volume, and O_2 is detected as the shoulder peak at retention time of 2.29 min. H_2 was measured with a 1 mL sampling volume for quantification and calculation purpose, and detected at 0.83 min retention time. 9.1 nmol H_2 was measured in the 1 mL sample volumn. A total headspace of 37 mL was used for the reaction cell, which leads to 0.337 µmol H_2 produced in total.

Supporting References

1. Bhattacharyya, B.; Pandey, A., CuFeS2 quantum dots and highly luminescent CuFeS2 based core/shell structures: synthesis, tunability, and photophysics. *Journal of the American Chemical Society* **2016,** *138* (32), 10207-10213.
2. Nakano, T.; Kikugawa, G.; Ohara, T., A molecular dynamics study on heat conduction characteristics in DPPC lipid bilayer. *The Journal of chemical physics* **2010,** *133* (15), 154705.
3. Ni, W.; Kou, X.; Yang, Z.; Wang, J., Tailoring longitudinal surface plasmon wavelengths, scattering and absorption cross sections of gold nanorods. *ACS nano* **2008,** *2* (4), 677-686.
4. Zhao, H.; Zhang, Y.; Zhang, X.; Qian, L.; Sun, M.; Yang, Y.; Zhang, Y.; Wang, J.; Kim, H.; Qiu, G., The dissolution and passivation mechanism of chalcopyrite in bioleaching: An overview. *Minerals Engineering* **2019,** *136*, 140-154.